The Polarization of Photons Produced in He$^+$ - He
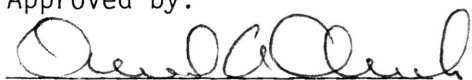Charge Transfer Collisions

by

Robert William Michaels
Department of Physics

Submitted in Partial Fulfillment of the Requirements of the
University Undergraduate Fellows Program

1980-1981

Approved by:

_____

Dr. David A. Church
Advisor

ABSTRACT

A method for measuring the vector polarization of collision-induced radiation is described and implemented. Studied in this research are the polarized de-excitations at 3889 $\overset{\circ}{A}$ characteristic of the 2^3S_1 - $3^3P_{2,1,0}$ transitions of helium atoms resulting from charge capture in low energy He^+ - He collisions. A qualitative extension of a recently advanced theoretical model, based on angular momentum transfer, appears to explain the experimental results.

ACKNOWLEDGEMENTS

TABLE OF CONTENTS

LIST OF FIGURES

INTRODUCTION

When no external torques act on a system, its total angular momentum is conserved; it follows that in ion-atom collisions, the sum of the angular momentum of the incident ion's trajectory motion and the internal angular momentum of the quasimolecular state, formed briefly ($\sim 10^{-15}$ seconds) during the collision of the ion and atom, is constant. Mono-energetic ions undergoing charge capture and scattering inelastically (i.e. some translational energy is invested in excitation) at an angle X (see figure 1), corresponding to an impact parameter b, may experience a change in trajectory angular momentum, $\vec{b} \times \vec{\Delta p_1}$, compensated by an electronic angular momentum change, which occurs resonantly in discrete units of h. The fast atom may therefore emerge in an excited state with net angular momentum, whose spatial orientation is quantized. When this unstable excited state decays back to its former angular momentum state, the unit of angular momentum is carried off by a spinning photon; in accord with wave-particle duality, this is equivalent to a circularly polarized electromagnetic wave, whose state of polarization can be described in terms of measureable Stokes parameters.

A recently published theory by A. Russek et. al.[1,2], based on the above model, describes the polarization effects associated with p to s electronic angular momentum transitions caused by collision induced excitations at a level crossing for ion-atom scattering in the keV range. In particular, the decrease in kinetic energy inherent to the subtle inelasticity of the collision is compensated by an increase in

2

FIGURE 1
View of Collision

Microscopic View

Macroscopic View

Before Collision

After Collision

He$^+$ (^{2}S)

$\Delta\vec{P_1}$

He(^{3}P)

X

$\Delta\vec{P_2}$

$\vec{R}$

$\vec{R}$

$\vec{K}$

b

He (^{1}S)
target atom

He$^+$ (^{2}S)

X

scattering plane

Charge is transferred.

K is perpindicular
to the plane.

FIGURE 2
Accelerator

He

High Voltage

Magnets

Int. Anode

Lens High Voltage

Optical
System

hot
filament

30 deg.

to diffusion
pump

Magnet

Collision
Chamber

to Diffusion
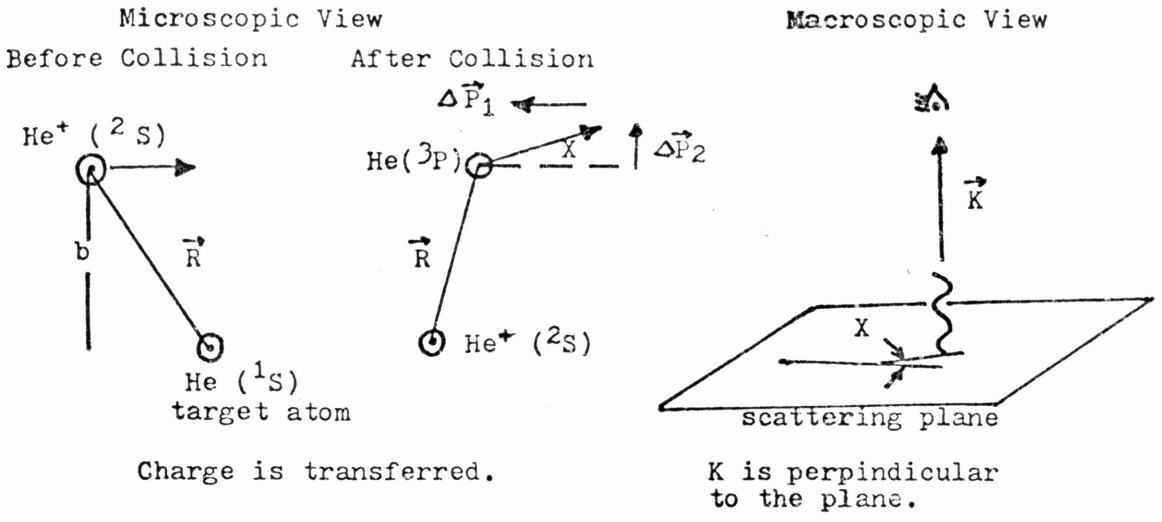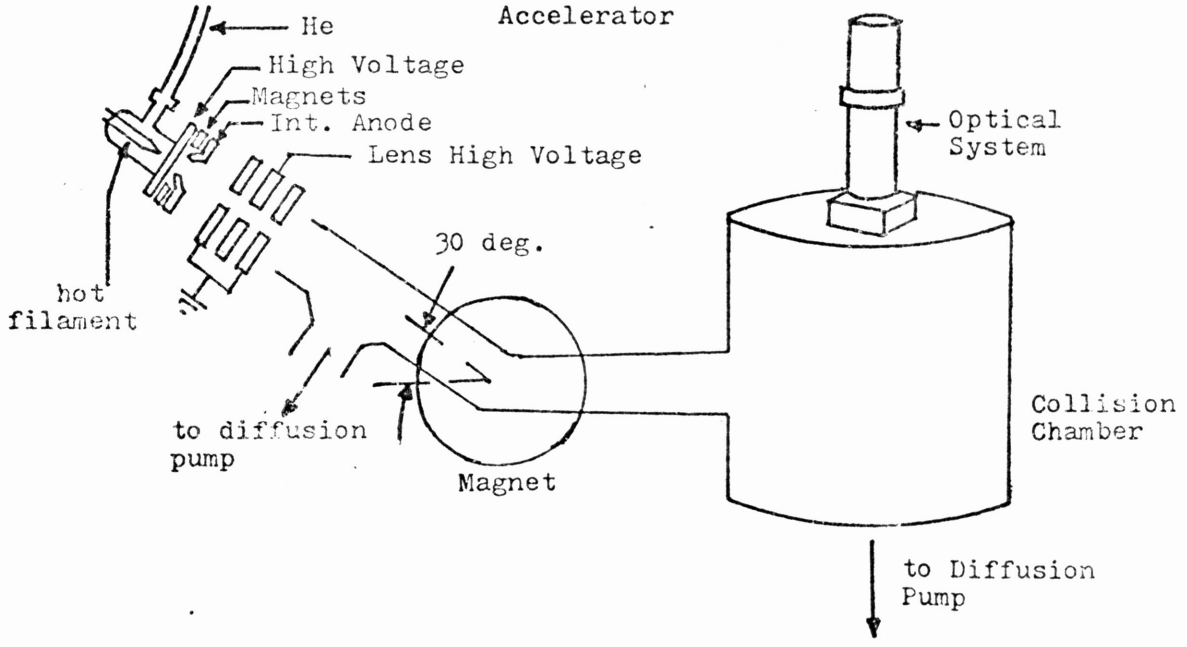Pump

the internal energy of the ion (or atom), i.e., an excitation by the amount of work $\Delta W = \langle \dot{\theta} \rangle \Delta L$ done on the internal degrees of freedom of the ion-atom system, where $\langle \dot{\theta} \rangle$ is the average angular velocity of $\vec{R}$ in figure 1 and where ΔL is the transfer of angular momentum from trajectory motion to the ion's S shell electron during excitation. By means of the energy level diagrams for the $He^+(^2S)$ + $He(^1S)$ system, the observable shift $\Delta \tau$ in the cross sections for right and left handed circularly polarized light (associated with positive and negative ΔL along the K axis in figure 1) may be predicted from this theory.

This thesis research studies experimentally the dependence of the circular polarization resulting in de-excitations of the $2^3S_1 - 3^3P_{2,1,0}$ transition of helium upon the reduced angle τ, a product of incident ion kinetic energy and scattering angle. The parameter τ is inversely proportional to b for small angle scattering.

One method for making this measurement, which has been employed successfully elsewhere[2], is to count photons in coincidence with scattered ions at an angle defined by collimating slits. Such a coincidence experiment was attempted for this measurement, but difficulties were encountered in ion detection. A new, relatively simple technique, which permits higher photon counting rates, has been designed and developed. This technique is a promising way to test the theory, and aspects of its operation can be compared with those reported by other researchers.[3,4]

APPARATUS

A. Accelerator

The accelerator served to create a focused, pure beam of mono-energetic ions, which for this experiment were helium ions. Figure two shows the accelerator, designed and constructed by G. Welch[5] and C. S. Lee[6]. Helium gas, at a pressure of 500 mtorr, enters through the stopcock and is ionized by a hot filament. With the magnets shown, the discharge ions are confined in cyclotron orbits to a small region between the anodes. The ion source and discharge power supply are floated at the extraction voltage, typically 2kV, by a Power Designs 1543 high voltage power supply and isolated from the laboratory's wall circuit with a 1 : 1 isolation transformer. The discharge power supply, an H.P. model 712B, and the filament current adjustment were safely housed in an insulated rack behind a clear lucite cover and were controlled with lucite rods.

Upon accelerating through the extraction potential, the ions are focused by a cylindrically symmetric electrical Einzel lens, which was biased by a Fluke model 410 B power supply. Source ions are deflected by an adjustable magnetic field perpindicular to the beam which, at the proper setting and together with a downstream aperture, selects helium ions on a charge to momentum basis. For two different singly charged ions, mass m_1 and m_2, of the same kinetic energy, the necessary condition to enter the collision chamber is that the radii of curvature of their trajectories in the magnetic field be equal. Thus one expects

that $\sqrt{m_1} / \sqrt{m_2} = i_1/i_2$, where i_1 and i_2 are the magnetic coil cur-
rents at which the respective ion currents are maximized in the colli-
sion chamber. With this, we established that the predominant ion cur-
rents observable were for helium and molecular nitrogen, as well as for
traces of hydrogen and oxygen.

B. Collision Chamber

To measure the polarization of radiation from scattered particles
at a particular scattering angle, we required a good vacuum region in
which the collisions between ions and target atoms could occur, plus a
technique for selecting the scattering angle of the fast particle with
a fair angular resolution. Following my advisor's suggestion, I have
designed and constructed a very simple, but useful method for doing
this, which is shown in figure 3.

The helium ion beam enters from the left in the figure and is
0.5 mm wide when it reaches the scattering center, which is 7.94 cm from
the center of the deflection plates. A positive voltage on the upper
plate in the figure establishes an electric field with which one can
deflect the ion beam by a desired amount. At the scattering center, a
stream of neutral helium atoms effuses from a hypodermic needle, whose
aperture is 0.30 mm in diameter. We placed the scattering angle selec-
tion slit 1.47 cm from the scattering center; its width was 0.18 mm,
making the angular resolution 0.70°.

In spite of our desire for high angular resolution, it was neces-
sary to place the selection slit fairly close to the scattering center
because the mean lifetime of the excited state leading to the transition
of interest was about 10^{-7} seconds, thus making the mean length over

FIGURE 3
Collision Chamber
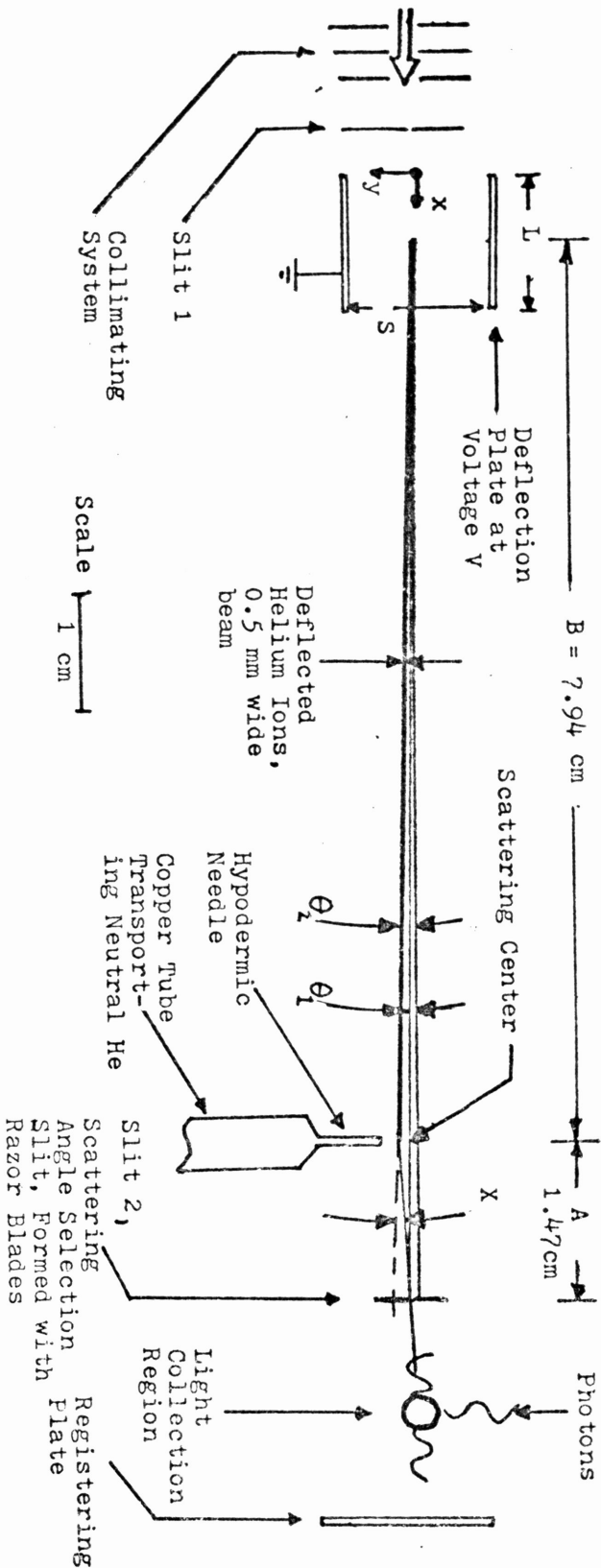
Helium ions enter on the left in the figure. A collimating system together with a 0.5 mm wide slit (slit 1) formed with razor blades defines the ion beam. The current on slit 1 is typically 2×10^{-7} amps. An electric field established across parallel plates deflects ions at some desired angle Θ. At θ_1 the beam is registered on the registering plate (far right). At θ_2 the scattering angle is X, as selected by a 0.18 mm wide slit (slit 2). The current on slit 2 is typically 3×10^{-8}. X is related to the necessary deflection voltage D, the deflection voltage V1 required for θ_1, and the accelerator voltage Va by:

$$X = 6.39 \left[\tan^{-1}\left(\frac{D}{2Va}\right) - \tan^{-1}\left(\frac{V1}{2Va}\right) \right]$$

which de-excitation occured about 3 cm for an ion energy of 2 keV. By
this we see that we must have the light collection region well within
3 cm of the scattering center.

Narrowing the selection slit to improve resolution imposed its own
disadvantage in that this was found to reduce the photon signal from
collision-induced excitations, which increases the amount of time re-
quired to count photons to attain an acceptable signal-to-noise ratio.

We can estimate the pressure in the atom source needle with a sim-
ple calculation. Let the pressure in the needle be P_N and the mean
pressure in the chamber be P_c. Denote the needle's conductance by C and
the diffusion pump's pumping speed by S. In equilibrium, $(P_N - P_c)C =$
SP_c. Evidently, $P_N >> P_c$, so that $P_N C = SP_c$. That is, $P_N = SP_c/C$. For
molecular flow the conductance can be estimated[7] from $\frac{80d^3}{(1 + 4d/3)}$ where

d is the diameter of the needle, 0.076 inches, 1 is the length of tube
in inches, .25 in, and where C is in units of liters/sec. This gives
C = 0.10 1/sec. The pumping speed of the diffusion pump is 2000 1/sec
and the experiment was run at typically $P_c = 4 \times 10^{-5}$ torr. (total oper-
ating pressures from 1 to 4×10^{-5} torr were used; the background pres-
sure was 2×10^{-6} torr.) Putting all this together gives $P_N \leq 0.8$
torr. The pressure just outside the orifice drops as r^{-2}, producing a
relatively small region where collisions occur with high probability.

The light collection region was a circle of radius 0.21 cm to the
right of the selection slit in figure 2. To prevent undesired light
arising from spurious de-excitations in the collision area from entering
the optical system, the region to the left of the selection slit was
covered on the sides and top with an aluminum baffel. Under otherwise

normal conditions (ion current at ~2 x 10⁻⁸ amps at the scattering center, average pressure 4 x 10⁻⁵ torr), only background light due to photomultiplier dark current pulses was registered when the selection slit was blocked.

The scattering angle is defined from the kinemantics associated with the deflection plates and from the chamber geometry. Consider figure 3, where the variables are defined. We shall first arrive at the deflection angle θ and then deduce the scattering angle X. The ions passing through the deflection plates feel a constant force in the y direction of magnitude qV/S, where q is the ion's charge and V is the voltage applied across the plates of separation S. Thus,

$$y = \frac{qv}{2mS} t^2$$

where t is the time progressing from the origin shown. With no force in the x direction, the velocity V_x is the constant ratio x/t. Thus,

$$y = \frac{qv}{2msV_x^2} x^2$$

Neglecting fringe effects, an ion stops accelerating when it reaches x = L and then moves tangentially from its previously parabolic flight. Hence, $\tan \theta = \frac{dy}{dx}\Big|_{x=L} = \frac{qVL}{msV_x^2}$

In this experiment L = S, and so

$$\tan \theta = \frac{qv}{mV_x^2}$$

The ions have kinetic energy $\frac{1}{2}mV_x^2 = qV_a$, where V_a is the accelerator voltage, so that $\tan \theta = \frac{V}{2V_a}$ or $\theta = \tan^{-1} \frac{V}{2V_a}$.

To get X, it is appropriate to employ a small angle approximation, setting $Ax = (A + B)(\theta_2 - \theta_1)$. θ_1 is the deflection angle, corresponding to some deflection voltage V_1, for which the ion beam runs straight through the selection slit and is registered on the plate downstream.

If we let D be the deflection voltage required to get a scattering angle X, then, by substituting the values for A and B, we get

$$x = 6.39 \left[\tan^{-1}\left(\frac{D}{2V_a} \right) - \tan^{-1}\left(\frac{V_1}{2V_a} \right) \right]$$

Just in terms of the ion beam width of 0.5 mm, we are actually accepting a range of scattering angles of about one degree centered about two degrees. Much like the earlier mentioned limitation, narrowing the beam reduces the photon count rate, in this case by reducing the collision rate. Nevertheless, this method has proved acceptable for our measurements. The spread of angles is shown by the error bars in our treatment of the results.

C. Optical System

The optical system, designed to collect light from scattered de-exciting atoms, is illustrated in figure 4. An aluminum cylinder is mounted on the collision chamber to place the bottommost quartz lens at its focal length, 1 5/8 inches, from the light collection region, which is the demagnified image of the photocathode of the photomultiplier tube. The aperture subtends a solid angle of 0.8 π steradians to the center of

FIGURE 4
Optical System

Light from de-exciting scattered atoms enters through the quartz window, progressing in turn through a filter, a $\lambda/4$ plate, and a linear polarizer. The lens system minimizes light losses. The photomultiplier detects individual photons.
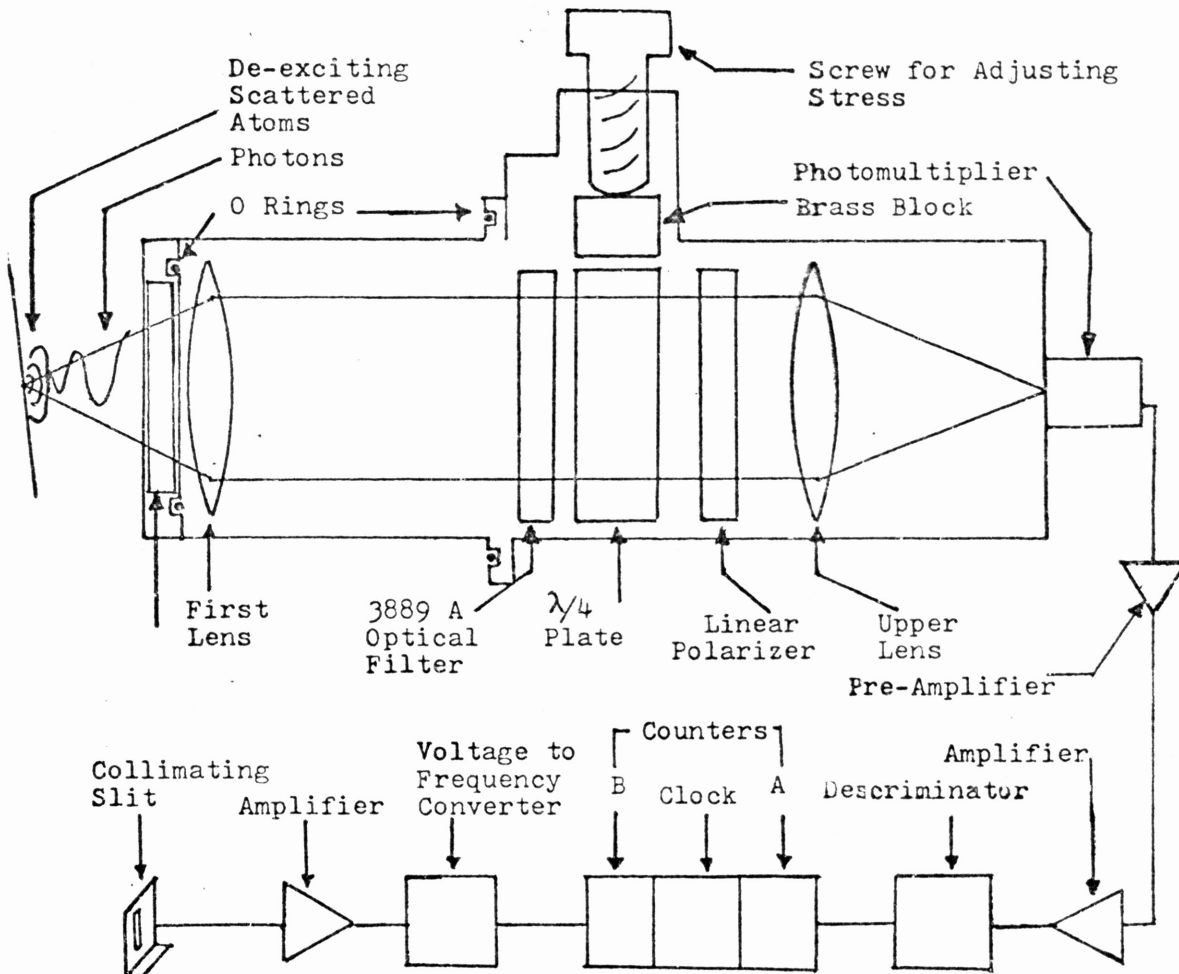
Only pulses above noise from the photomultiplier are passed by the descriminator and are subsequently counted. Ion current collected by a collimating slit is converted into an AC signal which clocks each photon counting cycle, thus normalizing to current fluctuations. A clock records the time interval of each cycle so that a constant rate background can be subtracted.

this circle.

The light from collisions emerges parallel from the first lens and passes through a plate of fused quartz, which when stressed serves as a quarter wave plate[5], and through a rotatable linear polarizer. These elements facilitate the measurement of the light polarization, analyzed in terms of the Stokes parameters. A filter selects 3889 $\overset{\circ}{A}$ light, characteristic of the 2^3S_1 - $3^3P_{2,1,0}$ transition of helium. The quartz lens on the top has a focal length of 5 inches, making the system's magnefication 3.08. The photomultiplier was an EMI - Gencom model 9789QB specially selected for low dark count rate.

The quartz plate can be made birefringent by applying a uniform stress along one face. Examining figure 4, one sees that when the screw is turned (with a torque wrench), the brass bar compresses the quartz block. The axis along the line of applied force is the fast axis.[5] To make measurements of linearly polarized light, we do not need a $\lambda/4$ plate so the quartz is not stressed; however, for circular polarization measurements we must apply the amount of torque necessary to retard the component of light along the slow axis by one quarter wavelength, which transforms circular to linear polarization, allowing it to be analyzed.

I have determined the amount of torque required to produce linearly polarized light from circularly polarized light at 3889 $\overset{\circ}{A}$ by determining the linear relationship between the torque required versus the wavelenght of incident light for our quartz block. The result is graphed in figure 5. Since the calibration was done in the visible region, it was important to verify that the linear fit extrapolated correctly to 3889 $\overset{\circ}{A}$, where we presume that 33.6 in-lbs will suffice. By shining linearly

polarized light onto the quarter wave plate at 45° to its fast axis, selecting only 3889 Å, and registering intensity with a photomultiplier, I found that 33.6 inch-lbs was the correct value of torque required to produce a $\lambda/4$ plate. Figure 6 shows the sum of squares of differences between intensities measured at four polarization angles versus the applied torque. Notice the minimum at 33.6 in-lbs.

The assembled system, with optical filter, was found to pass 3889 Å light with a full width at half maximum of 180 Å. The transmission was measured with a tunable monochromator.

The electronics used to count plates is diagrammed in figure 4. Photons incident on the cathode of the photomultiplier knock off electrons, which are accelerated through 1050 volts, successively striking intermediate dynodes where more and more electrons are liberated, producing a multiplying effect. Thus a photon is converted into a voltage pulse. These pulses are amplified immediately, to minimize losses, by an Ortec model 9301 preamplifier and then fed by 50Ω cable to an Ortec model 474 amplifier. An Ortec model 934 discriminator passes pulses above the Johnson noise; the discrimination level was set at 0.1 volts.

As will be discussed in VIII A, the photon count rate was found to be linear with the ion beam current producing it. It was consequently necessary to normalize the interval of time through which we count photons to the current. A Vidar model 260 voltage-to-frequency converter proportionally converts the voltage produced by collecting current at a collimating slit in the collision chamber into a frequency which is used to clock the photon counting cycle. To substract a constant rate component of background, the interval of time is simultaneously registered; the rate times time gives the background in a given cycle.

FIGURE 5
Quarter Wave Plate Calibration
Torque (T) versus Wavelength (λ)

Best Fit
$T = (.99)(\lambda/100) - 4.93$

Wavelength in Angstroms

FIGURE 6
Testing of Calibration
at 3889 A

Quarter Wave Condition
with 33.6 in-lbs
applied

Applied Torque (Inch-Lbs)
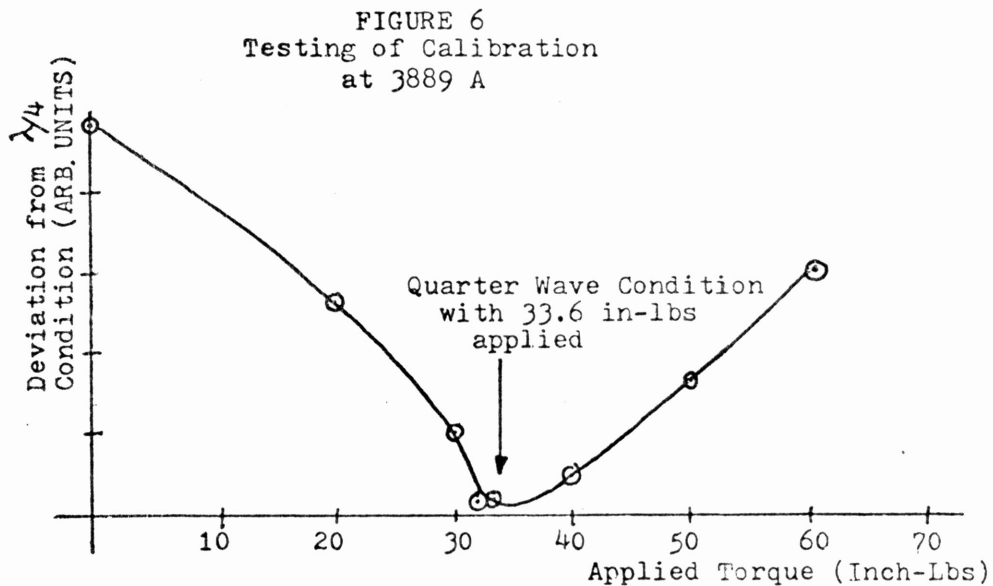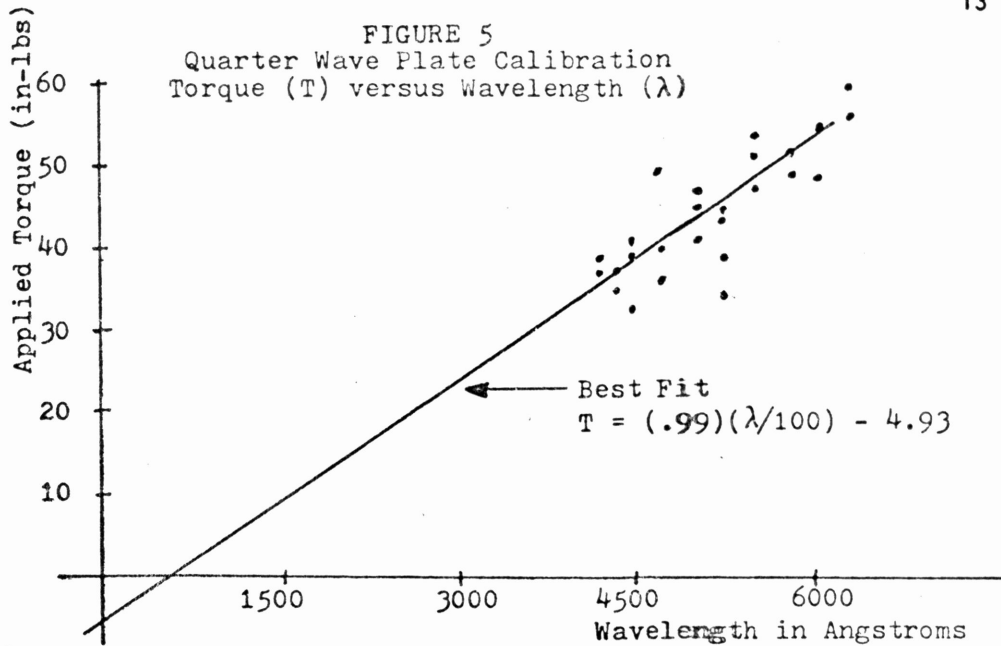
In testing the calibration, linearly polarized light was
shone on the stressed quartz at 45 degrees to the fast axis.
A true λ/4 plate will transmit circularly polarized light.
The sum of the squares of differences of transmitted inten-
sities (at 4 analyzer angles) with the average intensity
(over the 4 angles) is a measure of the deviation from the
λ/4 condition.

RECORD OF STUDY

A. Tests of Apparatus

In was important to test the newly assembled apparatus before attempting the proposed measurements. I was interested in knowing what wavelengths of light were produced by helium ion-atom collisions and in seeing how this signal depended on isolated variations in the parameters which are responsible for it - namely, ion current, target gas pressure, and scattering angle.

Figure 7 shows the frequency spectrum of the signal above background as well as the spectrum of background. We noticed a strong peak in the signal at 3889 $\overset{o}{A}$. This measurement used a 0.5 meter f/8.6 Jarrell-Ash model 82-000 Ebert Scanning Monochromator (with the 3889 $\overset{o}{A}$ filter removed) to select frequencies. The filament in the accelerator was found to contribute about forty percent of the background, which was rather surprising since the light from the hot filament has several apertures in its route to the photon collection region. Selecting a molecular nitrogen ion beam with the bending magnet, we saw the light spectrum of figure 8. These results gave us confidence that we were able to study the appropriate transition of helium at 3889 $\overset{o}{A}$.

Figure 9 demonstrates the linear dependence of the photon count upon ion current, illustrating the need to normalize the interval of time through which we count photons to a standard unit of charge impinging on the target. Figure 10 shows the linear dependence of the photon count rate upon the total collision chamber pressure, proportional to

FIGURE 7
Frequency Spectrum for He$^+$ - He

Definate Peak

Background
(no target
gas)

Signal above
background

3889 Å

Light Intensity (ARB UNITS)

3600 3700 3800 3900 4000 4100 4200 4300
Wavelength in Angstroms
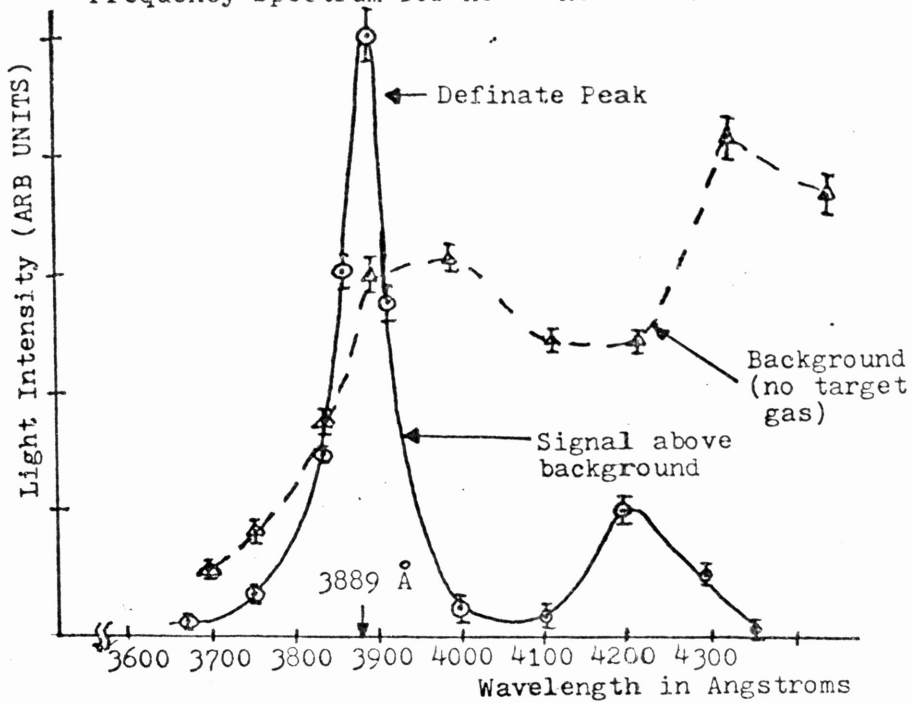
FIGURE 8
Frequency Spectrum for N$_2^+$ - CO$_2$

(Notice the absence of a
peak at 3889 Å.)

Light Intensity (ARB UNITS)

3600 3700 3800 3900 4000 4100 4200 4300
Wavelength in Angstroms
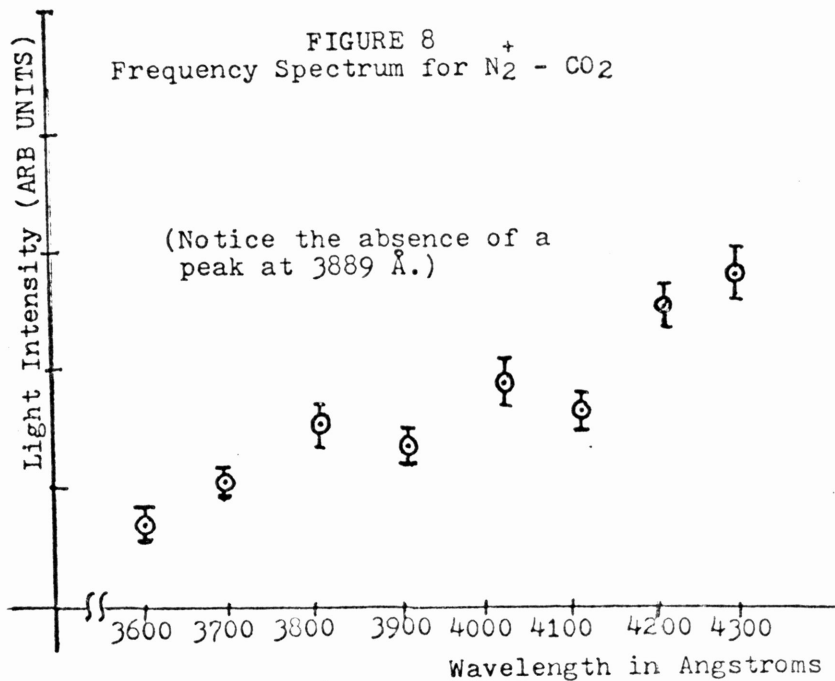
the target gas density, measured with a Consolidated Vacuum GIC-110A
ionization gauge. To guard against variations in pressure, we con-
structed a gas handling system which consisted of a high pressure stor-
age tank, an intermediate chamber, and a needle valve. A regulated flow
of helium emanates from the storage tank into an intermediate, vacuum-
tight chamber, where the gas reaches a constant pressure state. From
this chamber the gas flows to the collision chamber via copper tubing
and through a needle valve, which maintains a steady flow. We found
virtually no pressure fluctuations with this method. A similar system
was used to feed helium to the duoplasmatron souce of the accelerator.

The linear dependence of photon count rate on current and on target
pressure is quite plausible. We expect that under single collision con-
ditions the photon count rate to be given by

$$\frac{dN}{dt} = n_g \; \frac{I}{e} \; \sigma \; L \; d\Omega\gamma \; d\Omega p$$

where n_g is the density of the target atoms (which is proportional to
pressure), I is the ion current, e is the quantum of charge, σ is the
cross section for these collisions, L is a characteristic length along
the beam over which these collisions occur, $d\Omega\gamma$ is the solid angle which
our optical system accepts and $d\Omega p$ is a solid angle for scattered ex-
cited atoms. Substituting estimates for these values yields light
levels of the same order of magnitude as those observed. The main point
here is that the quantities I and n_g enter in a linear way, as observed.

We studied the dependence of light intensity upon the collision
impact parameter. The reader is reminded that, for small angle scatter-

Figure 9
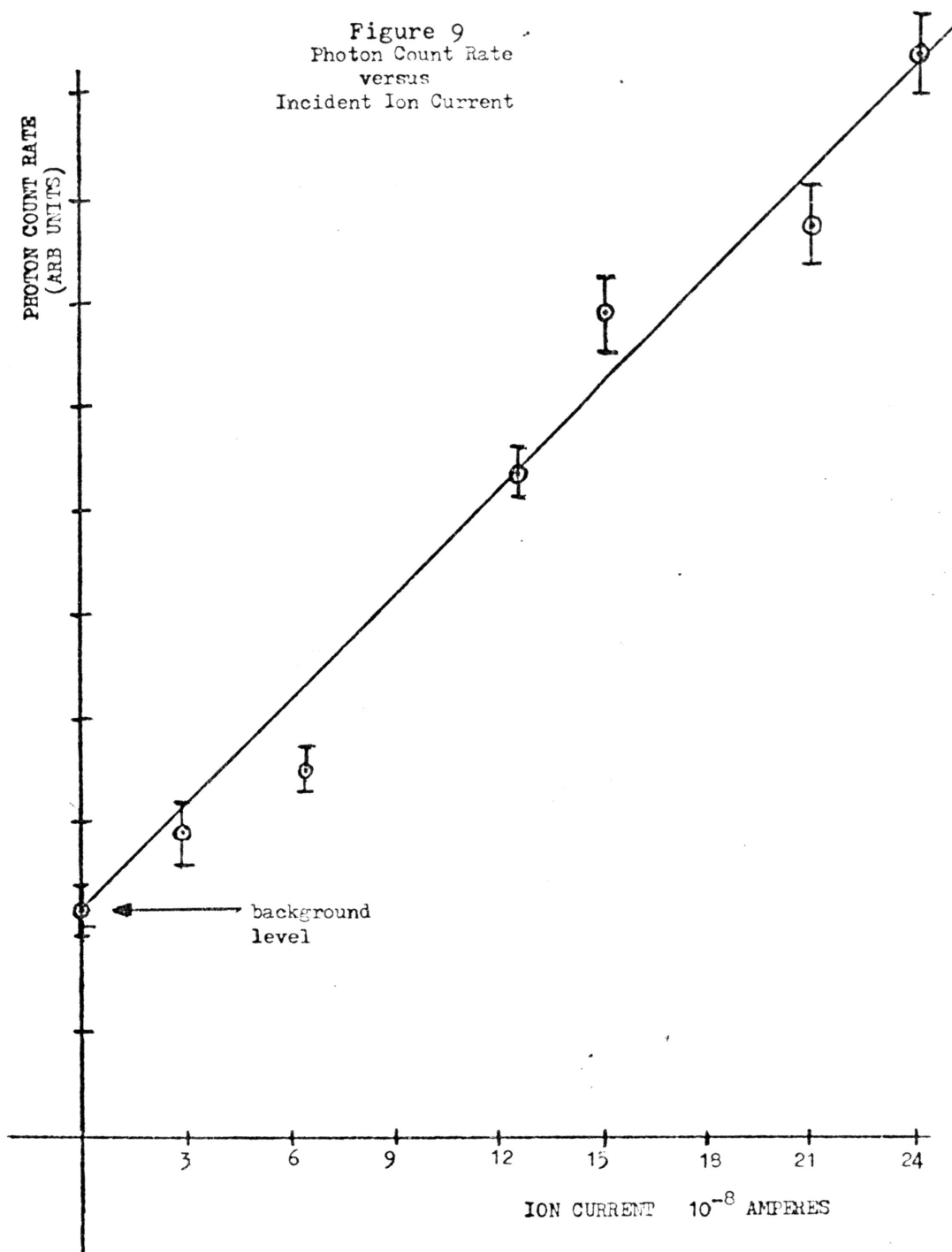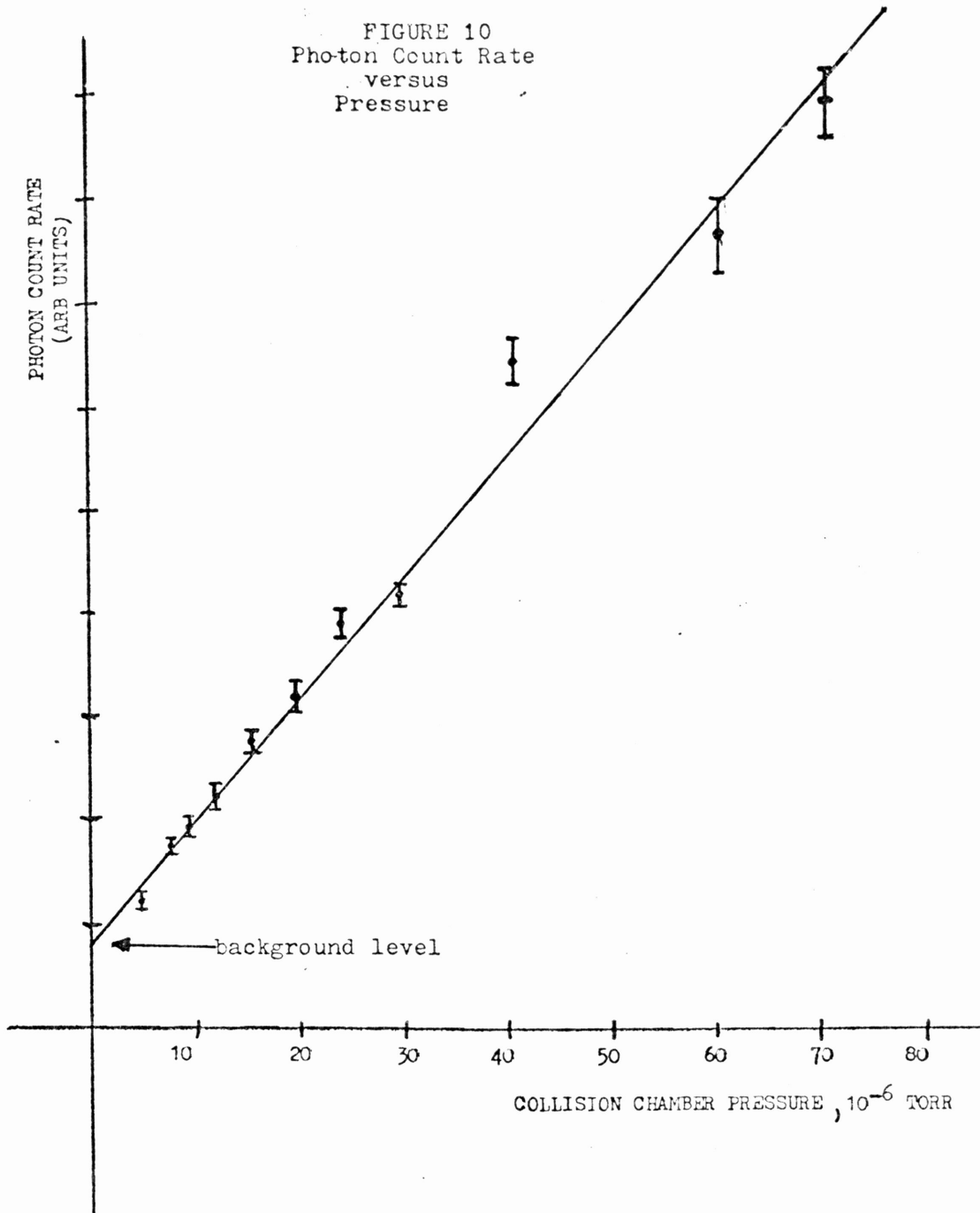Photon Count Rate
versus
Incident Ion Current

FIGURE 10
Photon Count Rate
versus
Pressure

PHOTON COUNT RATE
(ARB UNITS)

background level

COLLISION CHAMBER PRESSURE $, 10^{-6}$ TORR

10 20 30 40 50 60 70 80

For single scattering, one expects the photon count rate to
be linear with the gas density or pressure. Anderson[4] found
that his polarization measurements were pressure independent
for pressures below 1 mTorr in his apparatus. We took data at
pressures from 10 - 40 μTorr in this experiment.

ing, the impact parameter is inversely proportional to the reduced angle τ, a product of incident ion energy and scattering angle. Figure 11 shows a graph of the number of photons counted above background versus τ, while normalizing to ion current. The ion energy in this measurement was 2KeV. The fact that our selection slit geometry accepts a one degree wedge of scattered atoms explains the nonzero light intensity for the zero scattering angle on the plot. The results compare favorably to those of Eriksen, et al[3], who used the coincidence measurement technique. (Their experiment investigates the phase difference between scattering amplitudes for $m_1 = 0$ and $m_1 = 1$ magnetic sublevel formation.) The graph of their data is superimposed on ours. They study charge transfer excitation of 3.05 keV helium ions striking helium atoms, but measured only the linear polarization of the emitted radiation.

The tests described above gave us a fair indication that the newly constructed apparatus worked well; and, at first glance, our methods appear useful for making the vector polarization measurements detailed below.

B. Polarization Measurements

The measurement goal for this thesis research crystalized after several months of apparatus construction and preliminary investigations. The goal became determining the dependence of circular polarization upon the impact parameter, thereby leading to a more complete understanding of collision induced excitation. Only a few such measurements have been made and none previously for circulary polarized light production arising from charge capture at these energies.

With the description of the apparatus behind us, we are in a posi-

FIGURE 11
Photons Associated with Collisions
versus τ
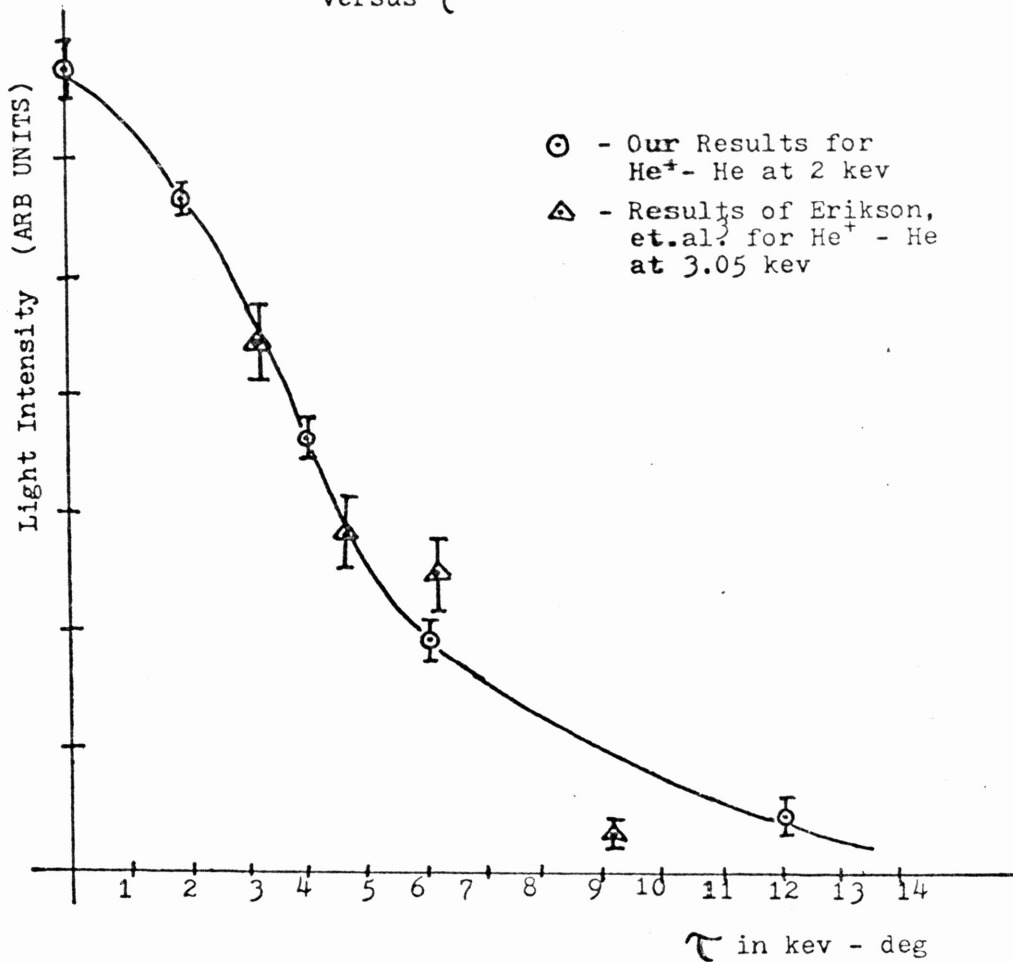
Our results, represented by the points with circles around them, are for the signal above background versus scattering angle at 2 kev. The results of Eriksen, et al[3], represented by the points with triangles over them, are based on the coincidence technique, in which photons are counted if and only if they coincide with a particle scattered at a particular angle.

tion to detail the theory of measurement. Figure 12 shows the view which our optical system has of the post-collision de-excitation process. Assume, for the sake of illustration, that a right hand circularly polarized photon enters the optical system vertically. The spinning photon, which is equivalent to a circularly polarized electromagnetic wave, impinges on the $\lambda/4$ plate. The verticle fast axis, along which the index of refraction is relatively small, advances the vertical component of the electric field by a $\pi/4$ phase shift. The emerging light is linearly polarized at 45°. With a little thought, one can see that right and left circularly polarized light lead to linear polarization intensity patterns at 45° and 135° to the fast axis, respectively.

The polarization measurements are summarized by figure 13, a plot of the third Stokes parameter, $P_3 = \dfrac{I(RHC) - I(LHC)}{I_{total}}$, versus τ. The curve through this data is not a theoretical curve; rather, it serves to guide the eye. The vertical error bars in the graph represent the upper and lower bounds of P_3 in terms of statistical error. The fluctuation $\sqrt{N}$ in the number of counts N representing an intensity can be added or subtracted, as appropriate, to get the limits in the quotient. The horizontal error bars represent the finite angular resolution of the apparatus.

One sees a certain symmetry about zero scattering angle. Since the experimental arrangement is asymmetric, perfect symmetry is not expected. For small positive angles (positive angles are left scattering), the light is somewhat right circularly polarized. We were initially surprised to see the light become predominantly left circularly polarized

FIGURE 12
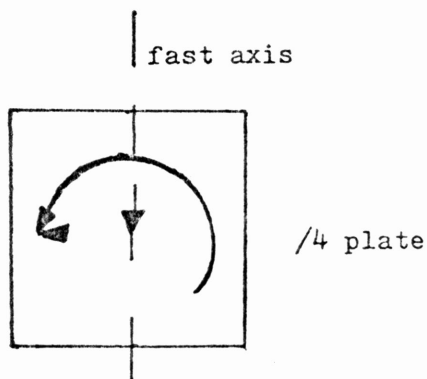### Optical System's View

A.   Incident RHC Light

B.   Emerging Linear Light
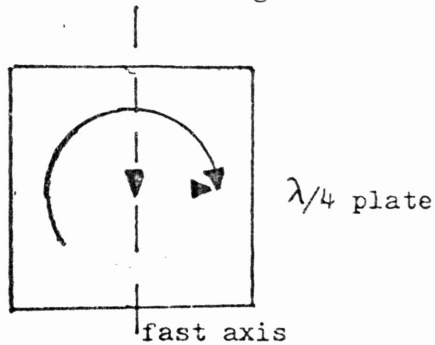
$\lambda/4$ plate
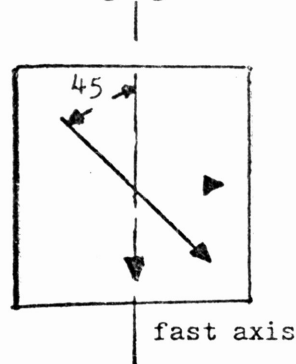
fast axis

fast axis

From the above picture one sees that RHC light incident on the $\lambda/4$ plate has its verticle E field component (along the fast axis) advanced by $\lambda/4$. This makes the components of figure A emerge in relative phase as shown in B, producing linearly polarized light which can be analyzed. Similar considerations pertain to LHC light, as represented below. In this figure, the LHC light becomes linearly polarized light at 135 degrees to the fast axis.

C. Incident LHC Light

D. Emerging Linear Light

fast axis

fast axis

$/4$ plate

FIGURE 13
P_3 versus τ

$$P_3 = \frac{I(RHC) - I(LHC)}{I_{total}}$$

LEGEND

▢ 2 kev, 40 μ Torr, Jan.
▽ 2 kev, 40 μ Torr, Mar.
⊘ 2 kev, 20 μ Torr, Mar.
♡ 2 kev, 40 μ Torr, Apr.
☆ 2 kev, 10 μ Torr, Apr.
△ 3 kev, 40 μ Torr, Apr.

Positive angles are left scattering.

τ in Kev-deg
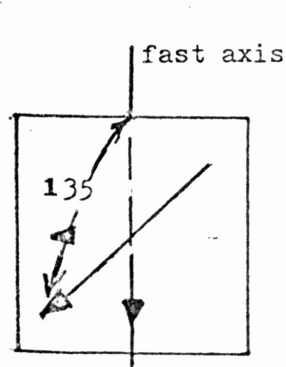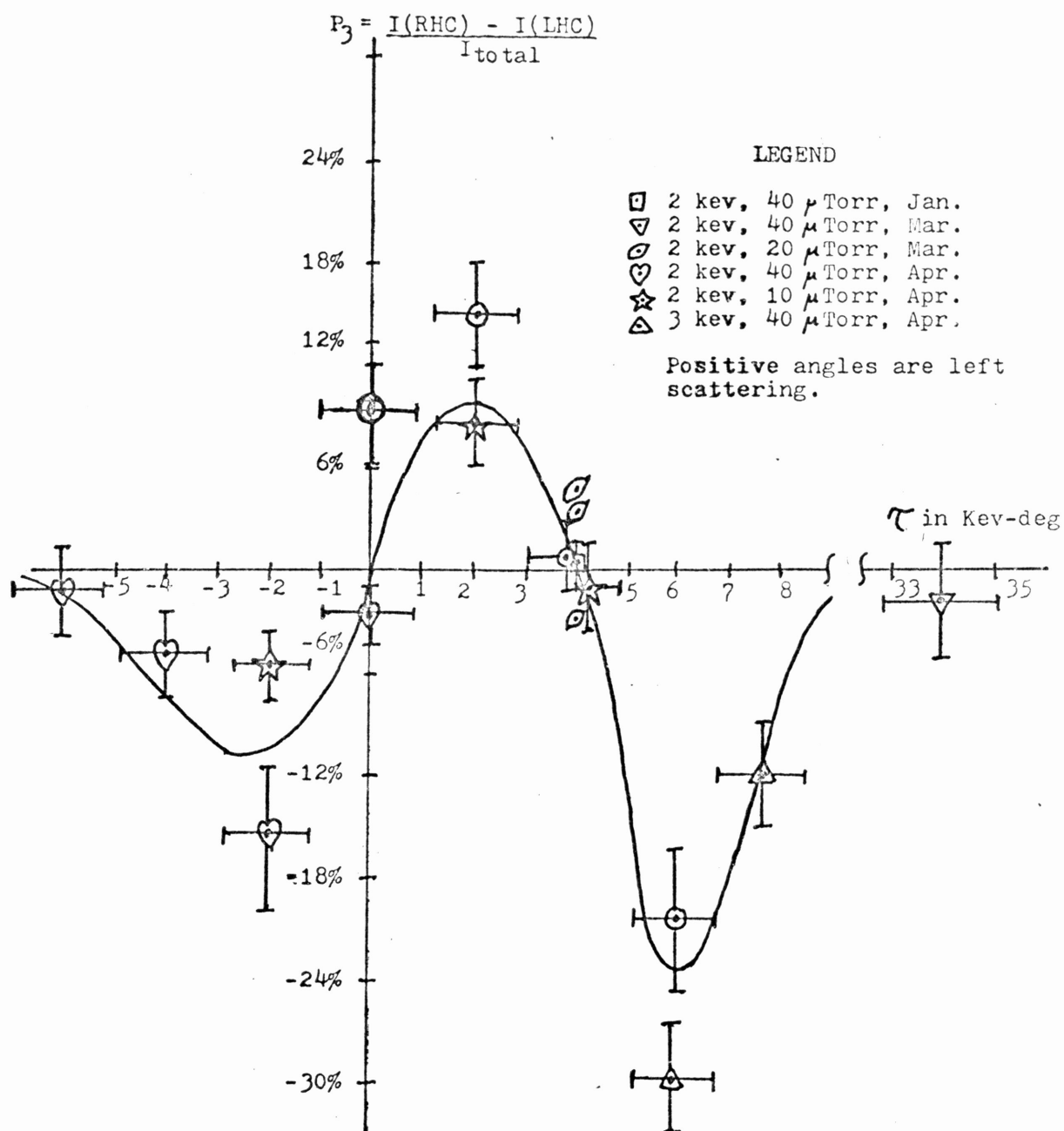
for larger values of τ, but we believe we can account for these effects in terms of an intuitively appealing, qualitative application of the new theory by Russek[1,2], which we now address.

C. Theoretical Interpretations and Conclusions

The recently published treatment by A. Russek, et al[1,2], of angular momentum effects in atom-atom scattering describes the formation of p+ and p- states in electronic excitations induced by collisions. For the purposes of explaining our data, we shall attempt to extend these considerations to charge capture, mingling in some of our own speculation.
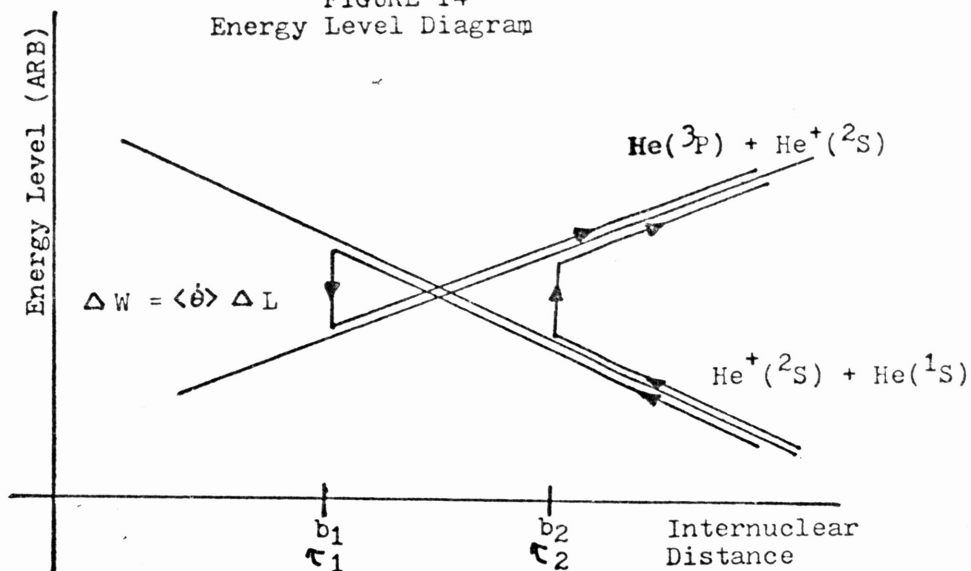
The explanation begins with the energy level diagrams for the quasimolecular states formed briefly, i.e. in about 10^{-15} seconds, by the collision process (see figure 14). In this diagram we see computer calculated electronic energy levels for two ion-atom systems. It is theorized that the jump from a He^+ (2S) state to an excited He (3P) state occurs in the vicinity of one of these curve crossings.

Let us consider scattering to the left. A discreet unit, $\hbar$, of trajectory momentum is transferred to the electronic angular momentum in the process. This is a consequence of work done, ΔW

$$\Delta L = \int T dt = \int T \frac{d\theta}{\dot{\theta}} = \frac{\Delta W}{<\dot{\theta}>}$$

That is, $\Delta W = <\dot{\theta}>\Delta L$, where $<\dot{\theta}>$ is the average angular velocity of rotation of the radial internuclear vector during the excitation. While there is some probability of excitation at any value of internuclear distance, it should be clear that the probability maximizes at the two impact parateters where the jump in energy is an amount ΔW compatible

FIGURE 14
Energy Level Diagram

$$\Delta W = \langle \dot{\theta} \rangle \Delta L$$

He(^{3}P) + He$^+$(^{2}S)

He$^+$(^{2}S) + He(^{1}S)

Energy Level (ARB)

b_1
τ_1

b_2
τ_2

Internuclear Distance

In these collisions the ion - atom system evolves from the lower right of this diagram and could emerge on the upper right. Of the many possible routes of evolution, two probable ones are shown, corresponding to the two impact parameters b_1 and b_2 .

FIGURE 15
View of Collision

For b_2

ΔP_1

ΔP_2

b_2

$\vec{\Delta L} = \vec{b} \times \vec{\Delta p_1}$ is $\odot$ (out of page)
electronic L is $\otimes$
photon is $\circlearrowright$ RHC

For b_1

ΔP_1

ΔP_2

b_1

$\vec{\Delta L} = \vec{b} \times \vec{p_2}$ is $\otimes$
electronic L is $\odot$
photon is $\circlearrowleft$ LHC
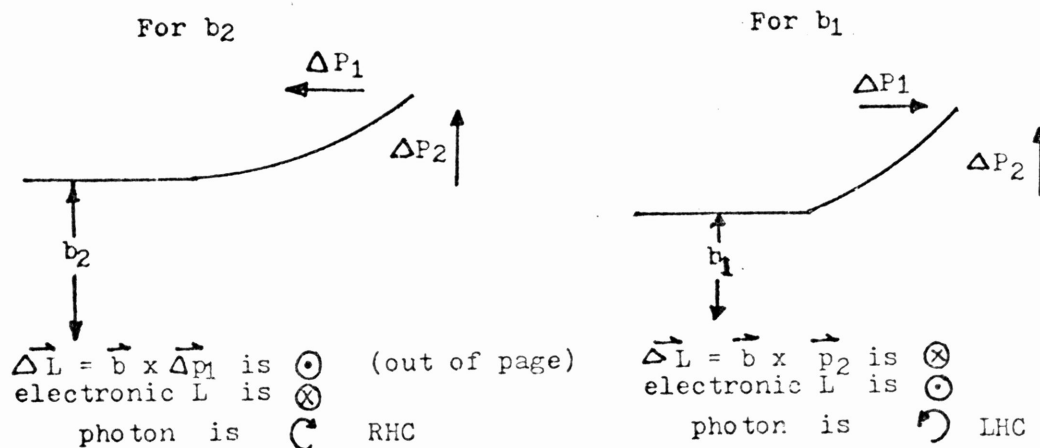
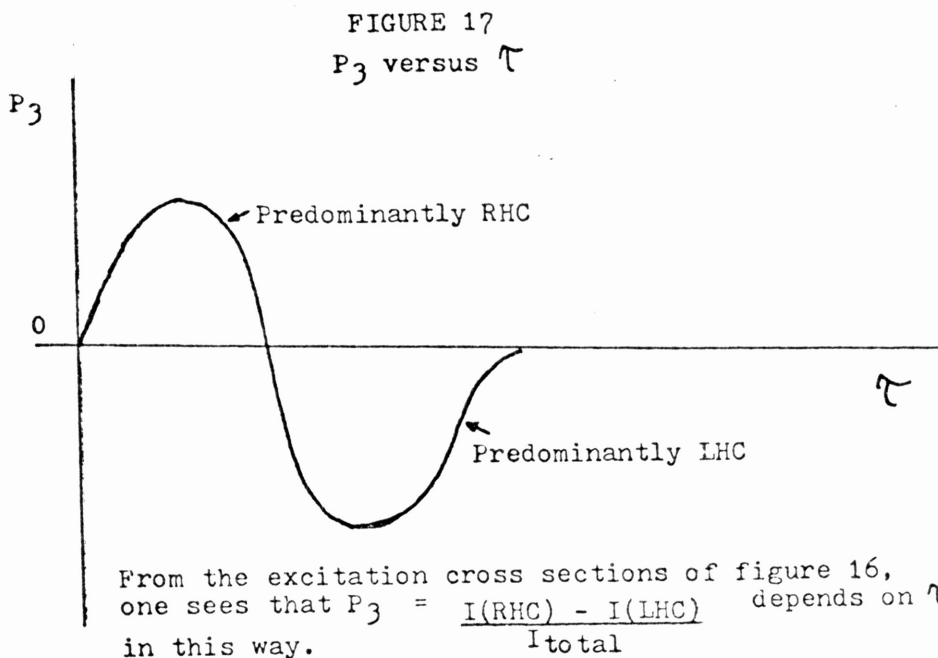with the discrete change ΔL in angular momnetum.

At impact parameter b_2, corresponding to τ_2, ΔW is positive. This is compensated by an abrupt retardation in the ion's kinetic energy which (see figure 15) amounts to a $\vec{\Delta L} = \vec{b_2} \times \vec{\Delta P_1}$ out of the page. Since angular momentum is conserved (i.e. the sum of trajectory angular momentum plus electronic angular momentum is constant), the electronic angular momentum must change in a direction into the page. When the excited state emits a photon, the photon carries away the angular momentum and the photon's sense of spin corresponds to right hand circularly polarized light[8], as observed at small τ (large b).

In a similar way, we can argue that an impact parameter b_1 the transition leads to left handed circularly polarized light. As seen in figure 14, we have the case that although the ion ultimately emerges in a higher energy state, the excitation process at b_1 occurs through a momentary decrease in electronic energy, compensated by a gentle forward kick felt by the ion undergoing excitation. Tracing through the arguement of the last paragraph, with all directions complementary, we deduce that this leads to LHC light preferentially emitted at large τ (small b). This process should have odd symmetry about zero scattering.

In terms of an excitation cross section, which one might think of as an ordinary cross section weighted by the probability of excitation, the above theoretical results lead to split maxima for RHC and LHC excitation, as shown in figure 16. These curves are based on my own qualitative interpretation of the theory; extensive computer calculations are required for each specific collision. Progressing positively from zero along the abscissa of the curve, one sees the variation of P_3 as depicted in figure 17.

FIGURE 16
Excitation Cross Section versus τ
(Interpretation of Theory)
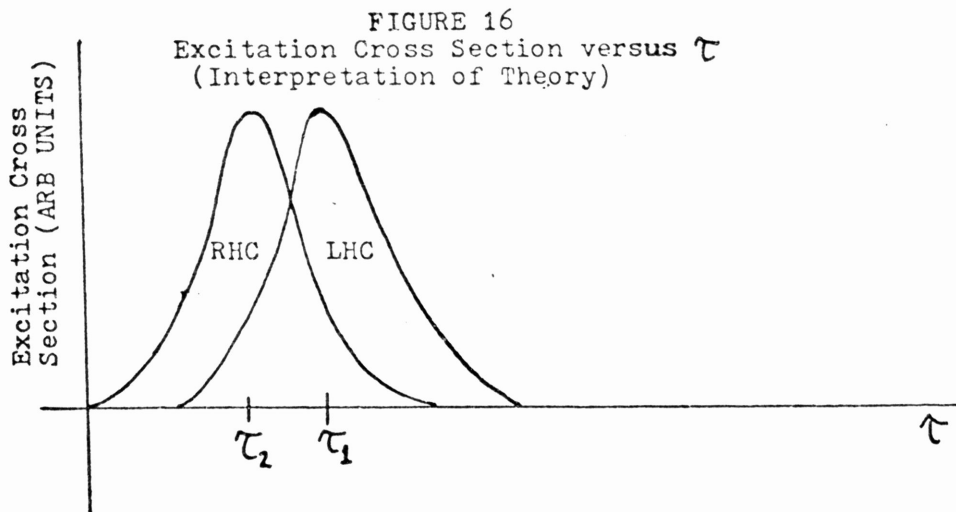
These excitation cross sections follow qualitatively from the considerations leading to figures 14 and 15.

FIGURE 17
P_3 versus τ

From the excitation cross sections of figure 16, one sees that $P_3 = \dfrac{I(RHC) - I(LHC)}{I_{total}}$ depends on τ in this way.

The reader should note the similarity between this qualitative graph and the empirical graph of figure 13.

This interpretation of Russek's theory seems to give a satisfactory qualitative explanation of our experimental results. To my knowledge, no other experimental investigations have suggested the extension of this theory to charge capture; it would appear, at least with our preliminary data, that the mechanism which excites the electron is irrelevant in this appealingly simple theory. However, deeper theoretical considerations and more extensive data collection will be necessary to support these qualitative assertions.

SUMMARY

I have designed and constructed a collision apparatus for the study of circularly polarized light arising from He^+ - He charge transfer collisions. Our tests of the new method have reasonably convinced us that we have met the prerequisites for making meaningful measurements: we see 3889 $\overset{o}{A}$ light from He^+ - He collisions, the light signal depends in a predictably linear way on ion current and target gas pressure, and the light intensity depends on τ in a way comparable to that found by other researchers.[3]

With this apparatus, we have measured the third Stokes parameter P_3 for various values of τ, as graphed in figure 13. No other measurements of this kind have been made. I have attempted to explain my data in terms of a recently published theory. My application of the theory, if substantiated, might extend the theory to low energy charge transfer collisions.

REFERENCES

1. A. Russek, Diffraction and Angular Momentum Effects in Semi-classical Atomic Scattering Theory, Phys. Rev. A 20, 1 (July 1979).

2. A. Russek, D. B. Kimball, Jr., and M. J. Cavagnero, Angular Momentum Effects in Atom-Atom Scattering, Phys. Rev. A 23, 1 (Jan., 1981).

3. F. J. Eriksen, D. H. Jaecks, W. deRijk, and J. Macek, Photon, Scattered-Atom Coincidence Measurements, with Polarization Analysis, in 3.0 kev He^+ - He Collisions, Phys. Rev. A 14, 1 (July 1976).

4. N. Andersen, T. Andersen, C. L. Cocke, and H. D. Pedersen, Differential-Excitation Studies of Quasi-One-Electron Systems II. Mg II 3^2P Alignment and Orientation in Mg^+ - He, Ne, Ar Collisions, J. Phys. B 12, 15 (1979).

5. G. Welch, Undergraduate Fellows Thesis, 1979.

6. C. S. Lee, Excited Level Anistropy Produced by Energetic Ion Interactions, 1980.

7. F. Rosebury, Handbook of Electron Tube and Vacuum Techniques, (Reading, Mass., Addison-Wesley Publishing Co., Inc., 1965), p. 217.

8. Hecht and Zajac, Optics (Reading, Mass., Addison-Wesley Publishing Co., Inc., 1979).